TiO_2/ZnO and ZnO/TiO_2 core/shell nanofibers prepared by electrospinning and atomic layer deposition for photocatalysis and gas sensing

Stefan I. Boyadjiev[1,2]*, Orsolya Kéri[3], Péter Bárdos[3], Tamás Firkala[3], Fanni Gáber[3], Zsombor K. Nagy[4], Zsófia Baji[5], Máté Takács[5,6], and Imre M. Szilágyi[2,3]

[1]*Institute of Solid State Physics, Bulgarian Academy of Sciences, 72 Tzarigradsko chaussee blvd., 1784 Sofia, Bulgaria*

[2]*MTA-BME Technical Analytical Chemistry Research Group, Szent Gellért tér 4, Budapest, H-1111, Hungary*

[3]*Budapest University of Technology and Economics, Department of Inorganic and Analytical Chemistry, H-1111 Budapest, Szent Gellért tér 4, Hungary*

[4]*Budapest University of Technology and Economics, Department of Organic Chemistry and Technology, H-1111 Budapest, Budafoki út 8, Hungary*

[5]*Hungarian Academy of Sciences, Research Centre for Energy, Institute of Technical Physics and Materials Science, H-1121 Budapest, Konkoly Thege M. út 29-33, Hungary*

[6]*Budapest University of Technology and Economics, Department of Physical Chemistry and Materials Science, H-1111 Budapest, Budafoki út 8, Hungary*

E-mail: boiajiev@gmail.com

Keywords: nanostructures; semiconductors; chemical synthesis; atomic layer deposition; catalytic properties; gas sensing

Abstract: In the present work, core TiO_2 and ZnO oxide nanofibers were prepared by electrospinning, then shell oxide (ZnO, TiO_2) layers were deposited on them by atomic layer deposition (ALD). The aim of preparing ZnO and TiO_2 nanofibers, as well as ZnO/TiO_2 and

TiO_2/ZnO nanocomposites is to study the interaction between the oxide materials when a pure oxide fiber is covered with thin film of the other oxide, and explore the influence of exchanging the core and shell materials on their photocatalytic and gas sensing properties.
The composition, structure and morphology of the pure and composite nanofibers were studied by SEM-EDX, TEM, XRD, FTIR, UV-Vis and Raman. The photocatalytic activity of the as-prepared materials was analyzed by UV-Vis spectroscopy through decomposing aqueous methyl orange under UV irradiation. The gas sensing of the nanofibers was investigated by detecting 100 ppm NH_3 at 150 and 220 °C using interdigital electrode based sensors.

1. Introduction

Semiconductor oxides are one of the most widely studied materials, due to their remarkable physical, optical and optoelectronic properties [1-2]. One approach to modify and improve the performance of a semiconductor oxide as a photocatalyst and gas sensing material is forming composite of it with other semiconductor oxides. Results from a number of previous researches reveal that many composite semiconductor oxides have better gas sensitivity and higher photocatalytic activity than a single semiconductor [3-5]. Another approach to improve the gas sensing and photocatalytic activity of these materials is to produce a nanostructured morphology to increase the surface area. Therefore, already various techniques have been adopted to fabricate nanostructured oxide materials. Among the reported nanostructures, nanofibers have received immense attention due to their high surface-to-volume ratio, combined with their good mechanical and physical properties [6-7]. Although, there are other methods for producing core/shell fiber nanocomposites [8], the technique including electrospinning of organic/inorganic fibers, consecutive calcination to form the core oxide nanofibers, combined with depositing shell layers on them by atomic layer deposition (ALD) is a powerful method to prepare composite oxide nanofibers with easily controllable parameters for various applications [9]. In our previous studies we already applied very thin ALD films for gas sensing [10-11], as well core/shell nanocomposite fibers produced by electrospinning and ALD to be successfully used as photocatalysts [12].
Electrospinning is one of the most widespread techniques for preparing metal oxide

nanofibers due to its simple set-up, high efficiency, low cost, reproducibility and good control of the diameter, morphology, composition and structure of the obtained materials [13-14]. It is a process by which fibers with diameters ranging from several nanometers to a few micrometers can be produced by applying an electric field by electrostatic charge-repulsion, stretching and thinning. In a typical process, a polymer solution or melt is injected from a small nozzle or micro-syringe pump under the influence of an electric field as strong as several kV/cm. The electrostatic charges on the surface of a liquid droplet induce the formation of a jet, which is subsequently stretched to form a continuous ultrathin fiber. In the continuous-feeding mode, numerous fibers can be formed within a very short time, creating fast and effectively a nanostructured material on the substrate.

ALD is a vapor phase deposition technique based on successive, alternating surface controlled and self-limiting reactions to produce highly conformal and uniform thin films with thickness control of sub-nanometer precision. By now ALD is capable to produce thin films of a large variety of materials. ALD also offers exceptional thin film conformality on high-aspect ratio structures and tunable film composition [15-18]. All these advantages make ALD a powerful tool for many industrial and research applications, and the method has constantly growing usage worldwide [19]. ALD is one of the most appropriate techniques for covering irregular surfaces and surface engineering high surface-area nanostructures, such as nanofiber matrices [18, 20-21].

Both titanium oxide (TiO_2) and zinc oxide (ZnO) are wide band gap n-type semiconductors, their band gap energies are similar to each other (approximately 3.2-3.4 eV), and they both possess good gas sensing and photocatalytic properties [1-3, 22-26]. Although, in the last decades the gas sensing and photocatalytic properties of both TiO_2 and ZnO nanofibers and thin films have been widely researched [3-5, 22-29], still there is a lack of knowledge about the gas sensing of core/shell nanocomposites, very thin films with thicknesses of a few nanometers and the influence of exchanging the core and shell materials on the gas sensing and photocatalytic properties. The fabrication of TiO_2/ZnO composite nanofibers and their gas sensing, photocatalytic activity, bactericidal properties and application in Li-Ion batteries have been reported more often previously [30-33], while the studies on core/shell composites of TiO_2 and ZnO are still quite limited [34-37].

In this study, we demonstrated the preparation of TiO_2 and ZnO, as well as TiO_2/ZnO and

ZnO/TiO_2 core/shell composite nanofibers by electrospinning and ALD and their possible application for gas sensing and photocatalysis. The as-obtained nanomaterials were characterized by SEM-EDX, TEM, XRD, FTIR, UV-Vis and Raman. The gas sensing was investigated by detecting 100 ppm NH_3 at 150 and 220 °C, while the photocatalytic properties were investigated by UV-Vis spectroscopy through decomposing aqueous methyl orange under UV irradiation.

2. Experimental methods

PVP/oxide organic/inorganic nanofibers were prepared through electrospinning using a home-made set-up. As feeding solution for the Ti-containing fibers a mixture containing polyvinylpyrrolidone [PVP, $(C_6H_9NO)_n$, K-90 by Merck], titanium tetraisopropoxide (TTIP, $Ti(O^iPr)_4$ by Sigma Aldrich), acetic acid (CH_3COOH, AcOH), and ethanol was used. 1 g TTIP was dissolved in 1 mL AcOH and 1 mL ethanol, stirred for 15 min, then added to 3 mL ethanol solution of 0.5 g PVP, and the whole mixture was stirred for 1 h before the electrospinning. For the Zn-containing fibers a mixture containing zinc acetate ($Zn(O_2CCH_3)_2$, Strem), PVP, ethanol and water was used. The 0.6 g ZnAc and 0.6 g PVP were dissolved in 2 mL distilled water and 3 mL ethanol, and then stirred for 1 h until a homogenous solution for the electrospinning process was obtained. The electrospinning was done at a characteristic distance of approximately 25 cm and the as-spun fibers were collected on an Al foil screen covered by a polyethylene foil. For the Ti-fibers 25 kV voltage and a feeding rate of 4 ml/h were used, while for the Zn ones the applied voltage was 20 kV and the feeding rate was 1 ml/h. In order to obtain pure TiO_2 and ZnO nanofibers, the as-prepared PVP/oxide fibers were heated to 550 ^oC in air with a rate of 1 °C min^{-1}, and held there isothermally for 1 h.

The covering of the fibers with thin films was accomplished using ALD deposition performed in a Picosun SUNALE R-100 reactor. The ZnO films were deposited at 200 ^oC using diethylzinc [$Zn(C_2H_5)_2$, DEZ] and H_2O as precursors. The TiO_2 films were deposited at 300 ^oC using TTIP and H_2O as precursors. The TTIP precursor was heated at 70 ^oC in order to reach sufficient partial pressure of its vapor. The overall pressure in the reactor chamber was ~10 mbar during both ZnO and TiO_2 depositions, and nitrogen was used as carrier gas. The precursor pulse times were 1 s for all of DEZ, TTIP and H_2O. The purge time

was 30 s after every precursor pulse. ZnO thin films were deposited in 25 ALD cycles, while for the TiO_2 films more time was needed to achieve a comparably homogenous layer over the fibers therefore 130 ALD cycles were used.

The film morphology was investigated by scanning electron microscopy (SEM) and the composition was studied by energy dispersive X-ray analysis (EDX) in a JEOL JSM-5500LV scanning electron microscope. Higher magnification SEM images were recorded by an FEI Inspect S50 SEM device. TEM images were taken by a FEI Morgagni 268 TEM microscope. FTIR spectra were measured between 400-4000 cm^{-1} by an Excalibur Series FTS 3000 (Biorad) FTIR spectrophotometer in KBr pellets. The XRD patterns were recorded by a PANalytical X'pert Pro MPD X-ray diffractometer using Cu Ka irradiation. Raman spectra were measured by a LabRAM system (Horiba Jobin-Yvon, Lyon, France) coupled with an external 532 nm Nd-YAG laser source (Sacher Lasertechnik, Marburg, Germany) and an Olympus BX-40 optical microscope (Olympus, Hamburg, Germany). An objective of 50×magnification was used for spectrum acquisition. UV-Vis reflection spectra were recorded by an Avaspec-2048 spectrophotometer.

The gas sensing properties of the nanofibers were investigated using a home-made setup. It contains a sandwich structured SiO_2/Si_3N_4 membrane with embedded Pt heater and gold interdigital electrodes on the top of the membrane. The Pt heater and the Au electrodes were positioned in the middle of the membrane. The membrane was prepared by deep reactive ion etching (DRIE) of Si underneath [38]. The tested nanofibers were dispersed in a mixture of ethylene glycol–water–ethanol and transferred onto the membrane of the sensor chip by drop coating. The as-transferred droplets were annealed at 200 ^oC for 10 min to remove the solvent. The sensors with the sensing nanofiber layers were tested in a flow-through chamber fed by mass flow controlled gases. All metal components, used in the electro-polished inner surfaces, were grounded in order to eliminate false signals. The sensors were tested with 100 ppm NH_3 in synthetic air at 220 °C and 150 °C operating temperatures. The sensor test was based on the measurement of the resistance change during the adsorption/desorption processes.

The photocatalytic activity of the samples was tested in the aqueous phase by decomposing methyl orange (MO). For this, 1 mg fiber sample was put into 3 mL aqueous 0.01 mM MO solution, kept in the dark for 1 h to adsorb dye, then illuminated by two parallel UV

backlights (Osram, 18 W). The UV-Vis spectra of the MO solutions were measured regularly during the photocatalytical reactions by a Jasco V-550 UV-VIS spectrophotometer. The absorbance values, which were proportional to the MO concentrations (according to the Lambert-Beer law), were determined at the MO absorption peak (463 nm). To have a correct comparison for each sample, relative absorbance A/A_0 values were calculated, where A_0 is the absorbance at the beginning of the photocatalysis reaction and A is the actual absorbance at the certain measurement point.

3. Results and discussion

The elaborated electrospinning process proved to be capable of high-speed quality production of Ti and Zn containing organic/inorganic PVP/TTIP and PVP/ZnAc fiber mats (Fig. 1a,b). After optimization of the electrospinning conditions, the obtained fibers were without nodes and defects. The electrospinning of ZnAc/PVP was more sensitive and needed longer tuning of the electrospinning conditions in order to obtain high-quality fibers. If the conditions (e.g. amount of ZnAc between 0.2-0.5 g, amount of EtOH between 0-2 mL, etc.) varied from the optimal ones, the fibers tend to form nodes (Fig. 1c) or aggregate (Fig. 1d). The size of the as-spun fibers in diameter was of about 300 nanometers (Fig. 1e), both for the Ti and Zn containing ones.

These organic/inorganic fibers were then calcined using a low heating rate of 1 °C min^{-1}. The very slow heating was needed to maintain the fibrous structure of the electrospun oxide materials, since it has been shown previously that the annealing of polymer/inorganic electrospun fibers at high heating rates leads to disintegration of the oxide fibers into particles [39]. The annealing of the PVP/inorganic fibers at 550 °C lead to formation of pure TiO_2 and ZnO fibers, which was proved by EDX, FTIR and Raman analysis. The fiber mats kept their shape and quality after the calcination process (Fig. 1f), and typical to electrospun oxide fibers they were composed of oxide nanoparticles [12]. The TiO_2 fibers (Fig. 2a) seemed to have smoother surface after the annealing, while the ZnO ones (Fig. 2b) had a rougher surface and were built up by larger particles. Both the TiO_2 and ZnO fibers shrunk during the calcination and were typically between 100 and 200 nm in diameter.

The FTIR analysis performed on the as-spun and calcined fibers showed (Fig. 3) that the polymer was effectively removed by annealing and was not present in the spectra of the

calcined fibers. The FTIR spectra of PVP/TTIP and PVP/ZnAc samples (Fig. 3a,c) were dominated by the bands of PVP. The broad peak at 3200-3600 cm^{-1} is the stretching vibration of the OH groups. The band at 2955 cm^{-1} can be explained by the CH stretching vibration of CH and CH_2. The highest intensity peak was the one at 1665 cm^{-1} which belongs to the C=O stretching vibration. The 1424 cm^{-1} band is the CH_2 bending vibration and the peak at 1290 cm^{-1} is the stretching vibrations of the C-O bonds [39]. The peak at 850 cm^{-1} can be assigned to the rocking vibration of the CH_3 groups in TTIP (Fig. 3a) [x1] and ZnAc (Fig 3c) [x2]. After annealing, the large peaks below 1000 cm^{-1} are typical lattice vibrations of the oxides (Fig. 3b,d).

The performed TEM imaging revealed that the TiO_2 fibers consisted of nanograins with size of about some nanometers (Fig. 4a), while the ZnO ones were built up by much larger nanoparticles with size of about tenths of nanometers (Fig. 4b). Such structures are both beneficial for photocatalysis and gas sensing, as the open structure of the fibers means higher specific surface area. It is hard only from the TEM images to conclude whether the TiO_2 or ZnO fibers have higher specific surface, but the nanostructured TiO_2 surface, which looked smoother on the lower resolution SEM images, was revealed to possess probably higher degree of roughness, while the ruffed-looking on the SEM images ZnO fibers seemed to have smoother surface.

Based on TEM images (Fig. 4c,d), after the ALD depositions constant oxide layers covered the fibers, thus successful preparation of core/shell nanocomposites was proved. It was observed that the ALD deposited ZnO thin film over the TiO_2 fibers was much thicker (Fig. 4c) than the ALD deposited TiO_2 film over the ZnO fibers (Fig. 4d). The thickness of the ZnO shell film is ~8 nm in average, while the TiO_2 shell is ~2 nm thick. From the images it was concluded that the ALD deposition of the ZnO film smoothened in high degree the surface of the core TiO_2 fibers, thus decreasing the specific surface area of the TiO_2/ZnO nanocomposite fibers. This smoothening effect was observed, but to a much smaller degree, when the thinner TiO_2 films grew over the ZnO fibers. This decreasing of the specific surface after the ALD deposition is supposed to influence negatively the photocatalytic and gas sensing properties of the nanocomposites, since the surface area is of high importance for both applications.

The EDX results, presented in Table I, confirmed the formation of the shell layers. From the

EDX results as well, it can be concluded that the ZnO shell over the TiO_2 fibers is considerably thicker than the TiO_2 shell on the ZnO fibers. Signals of carbon or nitrogen originating possibly from PVP impurities were not observed, which also proved the formation of pure inorganic fibers after the calcination process.

The XRD study (Fig. 5) showed that the calcined fibers were polycrystalline and in line with the literature. The TiO_2 fibers (Fig. 5a) crystallized as anatase, mainly in the (101) crystallographic orientation (PDF 00-021-1272). All typical peaks for crystalline ZnO were observed (Fig. 5c), corresponding to PDF 01-074-9940. The ZnO fibers also tended to crystallize preferentially in the (101) orientation. After investigating the TiO_2/ZnO composite fibers (Fig. 5b), besides reflections of TiO_2 we also found typical ZnO peaks, detected from the very thin ALD film, at 31.9^o (100) and 56.9^o (110). Also, the shelling effect was observed, as the intensity of the TiO_2 peaks decreased. For the ZnO/TiO_2 fibers (Fig. 5d) we could not find peaks from the ultra-thin TiO_2 film; however, it was already observed that in the case of core/shell fibers the shell oxide layers are hard to detect if they are thinner than 8-10 nm [12].

Raman investigations were also performed on both bare and composite nanofibers and their spectra were compared (Fig. 6). In the spectra of the clean TiO_2 fibers peaks can be observed at 395, 513 and 636 cm^{-1}, which can be assigned to the B_{1g}, A_{1g} or B_{2g} and E_g modes of the anatase phase [12], while the 446 cm^{-1} peak is the E_g mode of rutile TiO_2 [x3]. Though in XRD rutile could not be well detected besides anatase, Raman confirmed its presence. ZnO peaks from the shell layer of the TiO_2/ZnO fibers were hard to be detected, which was expected, as it was previously observed that very thin shell oxide films below 10 nm are hardly visible by Raman [12]. Nevertheless, it could be observed that the intensity and the position of the shoulder of the TiO_2 peak at 395 cm^{-1} changed, and based on this it could be identified as the most typical ZnO peak (437 cm^{-1}). The origin of the peak at 480 cm^{-1} cannot be clearly identified. Such peak was observed in epitaxially grown ZnO with nitrogen inclusions [40]. However, in our research nitrogen was only present as a constituent of PVP, and also as a purge gas during ALD reactions. The appearance of this peak is a surface effect, since it appears on the ZnO surfaces of both the bare ZnO and composite TiO_2/ZnO fibers (Fig. 6b,c). Such a peak is not observed on the spectra of TiO_2 and ZnO/TiO_2. This proves the presence of a continuous TiO_2 shell on ZnO core fibers, and that

this peak was an effect on the ZnO surface only, but not in the bulk. In the spectra of the clean ZnO fibers the peaks at 379, 437 and 577 cm^{-1} are the A_1(TO), E_2(high) and the A_1(LO) modes of crystalline ZnO [x4]. For the ZnO/TiO_2 fibers it was also difficult to find peaks from the ultra-thin TiO_2 shell; however, its presence could be assumed from the decreasing intensity of the ZnO signals and also from the small peak that appeared at 513 cm^{-1} (Fig. 6d).

From the UV-Vis spectra of the pure and composite nanofibers presented in Fig. 7 the absorption edges were determined, and based on them the band gap energies (E_g) were successfully calculated. E_g for the pure TiO_2 fibers was calculated as ~3.3 eV and for the ZnO ones it was ~3.13 eV. The UV-Vis spectra of the composites are close to the spectra of the core materials and shifted a bit towards the spectra of the shell material. This shift was well expressed for the TiO_2/ZnO composite, where E_g was determined as ~3.2 eV. For the ZnO/TiO_2 composite the shift from the bare ZnO fibers was minimal (differences in E_g ~0.01-0.02 eV), showing the rather small effect of the ultra-thin TiO_2 shell film on the E_g of ZnO.

The gas sensing properties of the nanocomposite fibers were studied by employing chips with interdigital electrodes on them (Fig. 8). Applying this method, we could study the gas sensing abilities of the nanofibers, which were deposited as a thin film on the testing electrodes by drop coating. In this coating method the amount of the deposited material on the electrodes cannot be precisely controlled; therefore, the gas sensing test is only qualitative and could give just approximate information how good the sensitivity of the material is towards the tested gas in certain temperature. For both the TiO_2/ZnO and ZnO/TiO_2 composite nanofibers we observed sensing response towards NH_3 at both 220 and 150 °C and absorption/desorption cycles with typical negative/positive changes. The TiO_2/ZnO fibers had larger response, which can be explained by that ZnO is considered to be a better gas sensing material than TiO_2. However, we found that the ZnO/TiO_2 composite fibers showed much faster response of only a few seconds, possibly due to that the TiO_2 film was much thinner than the ZnO shell in the case of the TiO_2/ZnO composite.

The results from the photocatalytic study, presented in Fig. 9, showed that the pure TiO_2 fibers possess the highest photocatalytic activity towards MO, followed by the pure ZnO fibers. This is according to what expected, since TiO_2 is considered to be a better

photocatalyst than ZnO. In contrast, the photocatalytic activity of both composite nanofibers decreased, compared to the pure fibers. Such results cannot be easily explained, but only taking the surface roughness and specific surface area of the catalysts into consideration. The voids between the particles of the oxides fibers were filled up to some extent by the ALD layers, and this decreased their specific surface. TiO_2 fibers seemed to possess the highest specific surface area due to their highly rough surface. But these nano-sized pores and cracks are easily filled up by the comparably thick ALD shell layer and the surface of the TiO_2/ZnO nanocomposite was much smoother, which led to lower specific surface area and considerable decrease in the photocatalytic ability, compared to the pure TiO_2 fibers. In the case of the ZnO fibers, the smoothening effect from the thinner ALD TiO_2 film was much smaller. Thus, the decrease of the specific surface of the ZnO/TiO_2 catalyst was weaker, and consequently a lower decrease in the photocatalytic activity was observed, compared to pure ZnO. It can be concluded that in the case of a nano-rough surface of an electrospun oxide fiber, the ALD grown shell layer should be ultra-thin, around 1 nm, in order the smoothening effect to be avoided or highly minimized, which was also observed in previous similar studies with core/shell nanocomposites [12].

Previously, it was shown that if the ALD shell layer is grown on an electrospun polymer/inorganic fiber, and the annealing comes only after that, then the photocatalytic activity of TiO_2/ZnO is also better than ZnO/TiO_2 core/shell nanofibers [36]. This fact was tried to be explained by Kayaci et al theoretically by electron-hole interactions between the core and the shell, while differences in the specific area of the materials were not taken into account. Now we have changed the preparation order to electrospinning/annealing/ALD, and received similar results. Since in [36] the photocatalytic activity of pure TiO_2 and ZnO fibers was not studied and comparison between bare and composite core/shell nanocomposites was not yet performed even by other authors, it is hard to conclude whether the electron-hole interactions between the core and the shell materials or the specific surface has stronger effect on the photocatalytic properties of TiO_2/ZnO and ZnO/TiO_2 core/shell nanocomposite fibers. But the negative smoothening effect of the ALD shell layers, which fill the voids between the particles in the fibers and thus reduce the photocatalytic activity, certainly have to be taken into account when highly effective photocatalysts are aimed to be prepared.

Probably, performing the calcination as a last step, preceded by the formation of the shell by ALD would benefit the final specific surface area of the fibers. But the annealing could have unpredictable impact over an ultra-thin ALD shell layer, e.g. formation of cracks can happen, and can practically cancel it as a continuous shell layer. On the other hand, depositing a thicker ALD film, which remains unaffected by the annealing as reported in [36], might decrease significantly the specific surface area and the photocatalytic activity as reported in [12], and also was found in the present research. Since such comparison studies with calcination both as middle and last steps were never performed previously, this could be a promising follow up of the present research.

4. Conclusions

Pure ZnO and TiO_2 nanofibers were obtained by electrospinning and annealing. Consecutively, by ALD several nanometer thick films from the other oxide were deposited on them, thus forming core-shell nanocomposite fibers. The properties of these nanocomposites were characterized by various methods (SEM-EDX, TEM, FTIR, Raman, UV-Vis), in order to study the formation of ultra-thin shells and their influence on the gas sensing and photocatalytic properties of the core material. The successful preparation of the pure and core/shell fibers was proved by SEM-EDX and FTIR. The formation of continuous shell layers over the fibers was observed by TEM and confirmed further by Raman spectroscopy. The crystalline nature of the pure fibers was shown by XRD, while the shift of the band gap of the nanocomposites caused by the shell layer grown on the core materials was determined by UV-Vis. The studied nanofiber composites were proved to be applicable for gas sensing and photocatalytic purposes. The TiO_2/ZnO composite had better gas sensing response, compared to ZnO/TiO_2; however, the influence of the thickness of the shell layer on response time was also observed. The electrospun oxide fibers were composed of a few nm particles, and the voids between them were partially filled by the shell ALD layers. This smoothening effect of the ultra-thin ALD shell was investigated, and its high importance on the specific surface area of the nanocomposites and consequently its strong influence on the photocatalytic properties were observed. It was shown that preparing nanocomposites by depositing shell ALD layers on electrospun oxide fibers decreased the photocatalytic activity due to reducing the active surface. Hence, deposition of as thin as possible shell

films is desired, in order not to reduce the specific surface area of the core fibers, and to obtain photocatalysts with optimal properties.

Acknowledgments

S. I. B. acknowledges the Postdoctoral Fellowship Programme of the Hungarian Academy of Sciences (2013-2015) and the INERA REGPOT Project of Institute of Solid State Physics, Bulgarian Academy of Sciences. I. M. S. thanks for a János Bolyai Research Fellowship of the Hungarian Academy of Sciences. An OTKA-PD-109129 grant is acknowledged.

References

1) A. Kołodziejczak-Radzimska, T. Jesionowski, Materials 7 (2014) 2833–2881.

2) U. Diebold, Surf. Sci. Rep. 48 (2003) 53–229.

3) R. Bogue, Sensor Rev. 34 (2014) 1–8.

4) D. L. Liao, C. A. Badour, and B. Q. Liao, J. Photochem. and Photobiology A: Chem. 194 (2008) 11–19.

5) H. Y. Wang, Y. Yang, X. Li, L. J. Li, C. Wang, Chin. Chem. Lett. 21 (2010) 1119–1123.

6) Y. Xia, P. Yang, Y. Sun, Y. Wu, B. Mayers, B. Gates, Y. Yin, F. Kim, H. Yan, Adv. Mater. 15 (2003) 353–389.

7) I. M. Szilágyi, D. Nagy, J. Phys. Conf. Ser. 559 (2014) 012010.

8) X. Peng, A. C. Santulli, E. Sutter, S. S. Wong, Chem. Sci. 3 (2012) 1262–72.

9) E. Santala, M. Kemell, M. Leskelä, M. Ritala, Nanotechnology 20 (2009) 035602.

10) S. Boyadjiev, V. Georgieva, L. Vergov, Z. Baji, F. Gáber, I. M. Szilágyi, J. Phys. Conf. Ser. 559 (2014) 012013.

11) S. I. Boyadjiev, V. Georgieva, R. Yordanov, Z. Raicheva, I. M. Szilágyi, Appl. Surf. Sci. 387 (2016) 1230–1235.

12) I. M. Szilágyi, E. Santala, M. Heikkila, V. Pore, M. Kemell, T. Nikitin, G. Teucher, T. Firkala, L. Khriachtchev, M.Rasanen, M. Ritala, M. Leskela, Chem. Vapor Dep. 19 (2013) 149–155.

13) B. Ding, J. Yu, Electrospun Nanofibers for Energy and Environmental Applications. Springer, Heidelberg, 2014.

14) D. Li, Y. Xia, Adv. Mater. 16 (2004) 1151–1171.

15) Steven M. George, Chem. Rev. 110 (2010) 111–131.

16) M. Leskelä, M. Ritala, Angew. Chem. Int. Ed. 42 (2003) 5548–5554.

17) V. Miikkulainen, M. Leskelä, M. Ritala, R. L. Puurunen, J. Appl. Phys. 113 (2013) 021301.

18) R. W. Johnson, A. Hultqvist, S. F. Bent, Mater. Today 17, (2014) 36–46.

19) R. L. Puurunen, Chem. Vapor Dep. 20 (2014) 1–13.

20) M. Liu, X. Li, S. K. Karuturi, A. I. Y. Tokb, H. J. Fan, Nanoscale 4 (2012) 1522–1528.

21) I. M. Szilágy, G. Teucher, E. Harkonen, E. Farm, T. Hatanpa, T. Nikitin, L. Khriachtchev, M. Rasanen, M. Ritala, and M. Leskelä, Nanotechnology 24, 245701 (2013).

22) J. Bai, B. Zhou, Chem. Rev. 114 (2014) 10131–10176.
23) A. L. Linsebigler, G. Lu, J. T. Yates Jr., Chem. Rev. 95 (1995) 735–758.
24) K. Hashimoto, H. Irie, A. Fujishima, Jpn. J. Appl. Phys. 44 (2005) 8269–8285.
25) U. Ozgur, D. Hofstetter, H. Morkoc, Proc. IEEE 98 (2010) 1255–1268.
26) A. A. Khodja, T. Sehili, J.-F. Pilichowski, P. Boule, J. Photochem. Photobiol. A 141 (2001) 231–239.
27) B. Ding, M. Wang, J. Yu, G. Sun, Sensors 9 (2009) 1609–1624.
28) P. Du, L. Song, J. Xiong, H. Cao, J. Mater. Sci. 48 (2013) 8386–8392.
29) S. J. Doh, C. Kim, S. G. Lee, S. J. Lee, H. Kim, J. Hazard. Mat. 154 (2008) 118–127.
30) Y. Wang, W. Jia, T. Strout, A. Schempf, H. Zhang, B. Li, J. Cui, Y. Lei, Electroanalysis 21 (2009) 1432–1438.
31) R. Liu, H. Ye, X. Xiong, H. Liu, Mater. Chem. Phys. 121 (2010) 432–439.
32) S. H. Hwang, J. Song, Y. Jung, O. Y. Kweon, H. Song, J. Jang, Chem. Commun. 47 (2011) 9164–9166.
33) M. A. Kanjwal, N. A. M. Barakat, F. A. Sheikh, H. Y. Kim, Bioceram. Develop. App. 1 (2011) D11012.
34) J. Y. Park, S.-W. Choi, J.-W. Lee, C. Lee, S. S. Kim, J. Am. Ceram. Soc. 92 (2009) 2551–2554.
35) M. E. Fragalá, I. Cacciotti, Y. Aleeva, R. L. Nigro, A. Bianco, G. Malandrino, C. Spinella, G. Pezzotti, G. Gusmano, Cryst. Eng. Comm. 12 (2010) 3858–3865.
36) F. Kayaci, S. Vempati, C. Ozgit-Akgun, I. Donmez, N. Biyikli, and T. Uyar, Nanoscale 6 (2014) 5735–5745.
37) D. Shao, H. Sun, G. Xin, J. Lian, and S. Sawyer, Appl. Surf. Sci. 314 (2014) 872–876.
38) M. Takács, C. Dücső, A. E. Pap, Sens. Actuators B 221 (2015) 281–289.
39) I. M. Szilágyi, E. Santala, M. Heikkilä, M. Kemell, T. Nikitin, L. Khriachtchev, M. Räsänen, M. Ritala, M. Leskelä, J. Therm. Anal. Calorim. 105 (2011) 73–81.
40) K. H. Ahn, Y. B. Park, D. W. Park, Surf. Coat. Techn. 171 (2003) 198-204.
41) I. Uslu, B. Baser, A. Yayli , M. L. Aksu, e-Polymers 145 (2007) 1-6.
42) T. Mazza, E. Barborini, P. Piseri, P. Milani, D. Cattaneo, A. Li Bassi, C. E. Bottani, C. Ducati, Phys. Rev. B 75 (2007) 045416-1-045416-5.
43) S. Lautenschläger, S. Eisermann, B. K. Meyer, G. Callison, M. R. Wagner, A. Hoffmann,

Phys. Status Solidi (RRL) 3 (2009) 16–18.
44) B. Hadzic, N. Romcevic, D. Sibera, U. Narkiewicz, I. Kuryliszyn-Kudelska, W. Dobrowolski, M. Romcevic J. Phys. Chem. Solids 91 (2016) 80-85.

Table I. EDX study of TiO_2/ZnO and ZnO/TiO_2 composite nanofibers.

Element	TiO_2/ZnO		ZnO/TiO_2	
	Atomic%	Weight%	Atomic%	Weight%
O	61.0	30.9	57.2	25.0
Ti	21.1	32.0	40.0	71.3
Zn	17.9	37.1	2.8	3.7

Figure Captions

Fig. 1. SEM images of electrospun nanofibers: a) TTIP/PVP fibers; b) ZnAc/PVP fibers; c) Node formation in ZnAc/PVP fibers; d) Aggregations in ZnAc/PVP fiber mats; e) Diameter measurement of ZnAc/PVP fibers; f) ZnAc/PVP fiber mats after annealing.

Fig. 2. High resolution SEM images of electrospun nanofibers after calcination: a) TiO_2 fibers; b) ZnO fibers.

Fig. 3. FTIR spectra of as-spun and calcined nanofibers: a) PVP/TTIP fibers; b) TiO_2 fibers obtained by annealing PVP/TTIP; c) PVP/ZnAc fibers; d) ZnO fibers obtained by annealing PVP/ZnAc.

Fig. 4. TEM images of bare and composite nanofibers: a) TiO_2 fiber; b) ZnO fiber, c) TiO_2/ZnO fiber; d) ZnO/TiO_2 fiber.

Fig. 5. XRD patterns of bare and composite nanofibers: a) TiO_2 fibers; b) TiO_2/ZnO fibers; c) ZnO fibers; d) ZnO/TiO_2 fibers.

Fig. 6. Raman spectra of bare and composite fibers: a) TiO_2; b) TiO_2/ZnO; c) ZnO; d) ZnO/TiO_2 nanofibers.

Fig. 7. UV-Vis spectra of bare and composite TiO_2; TiO_2/ZnO; ZnO and ZnO/TiO_2 nanofibers.

Fig. 8. Gas sensing tests of the composite nanofibers towards 100 ppm NH_3:
a) Gas sensing of TiO_2/ZnO fibers at 220 °C; b) Gas sensing of ZnO/TiO_2 fibers at 220 °C;
c) Gas sensing of ZnO/TiO_2 fibers at 150 °C.

Fig. 9. Photocatalytic activity of the bare and composite TiO_2; TiO_2/ZnO; ZnO and ZnO/TiO_2 nanofibers.

Figures

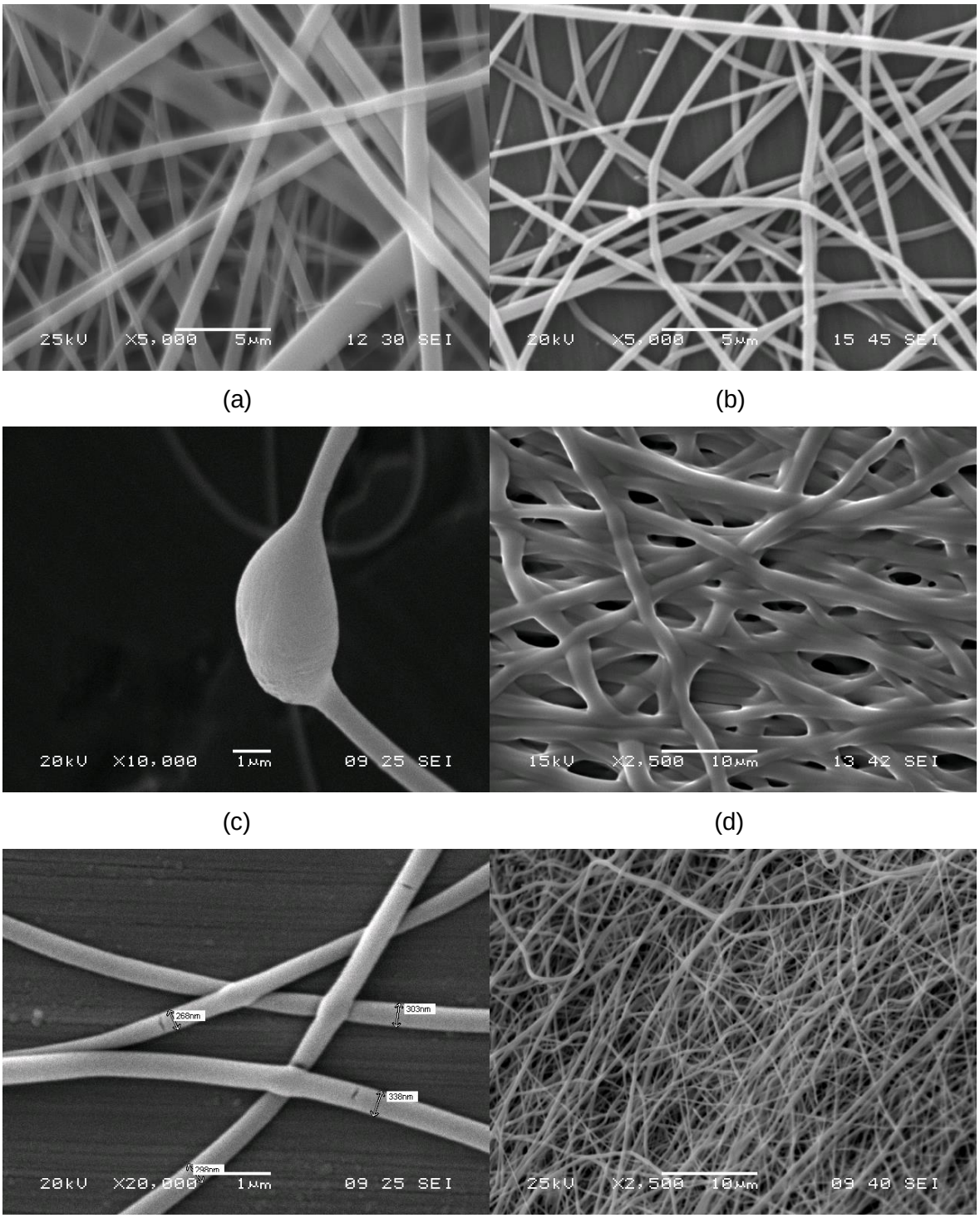

Fig. 1.

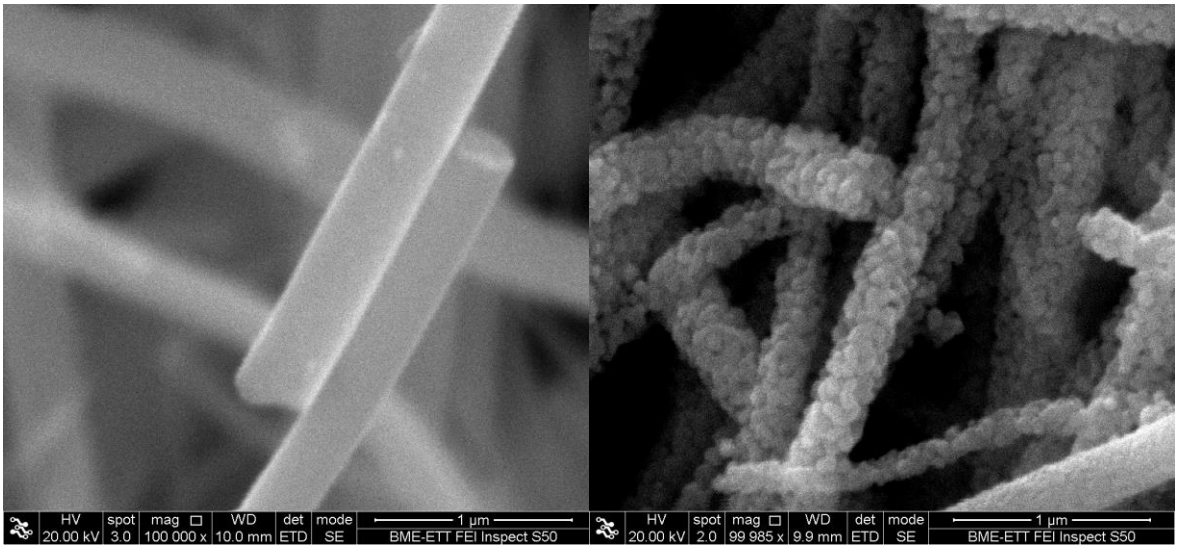
HV
20.00 kV
spot
3.0
mag
100 000 x
WD
10.0 mm
det
ETD
mode
SE
1 µm
BME-ETT FEI Inspect S50
HV
20.00 kV
spot
2.0
mag
99 985 x
WD
9.9 mm
det
ETD
mode
SE
1 µm
BME-ETT FEI Inspect S50

(a) (b)

Fig. 2.

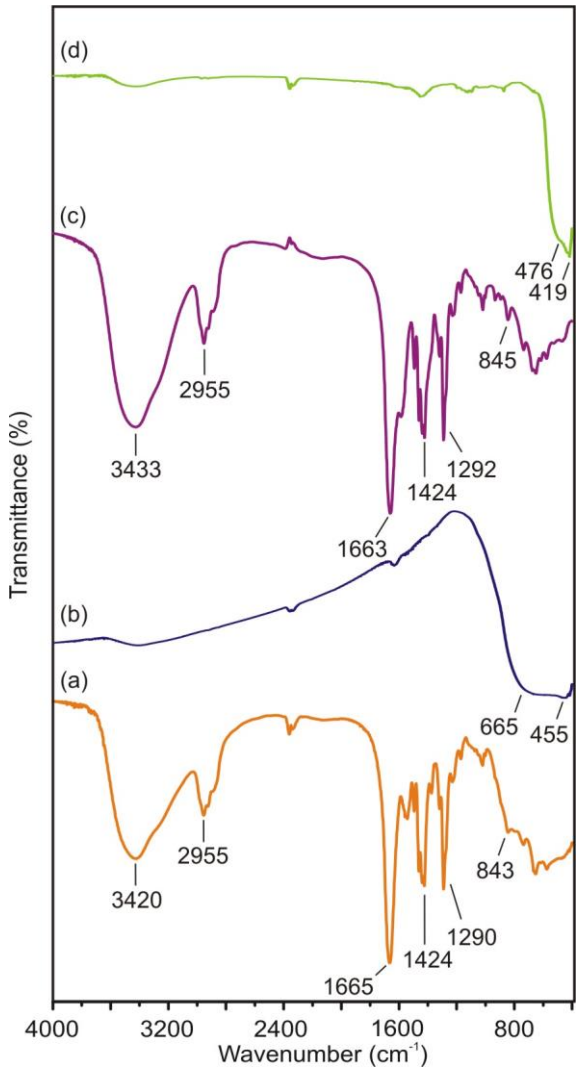
(d)
(c)
(b)
(a)
476
419
845
2955
3433
1292
1424
1663
665
455
2955
843
3420
1290
1424
1665
Transmittance (%)
4000
3200
2400
1600
800
Wavenumber (cm-1)

Fig. 3.

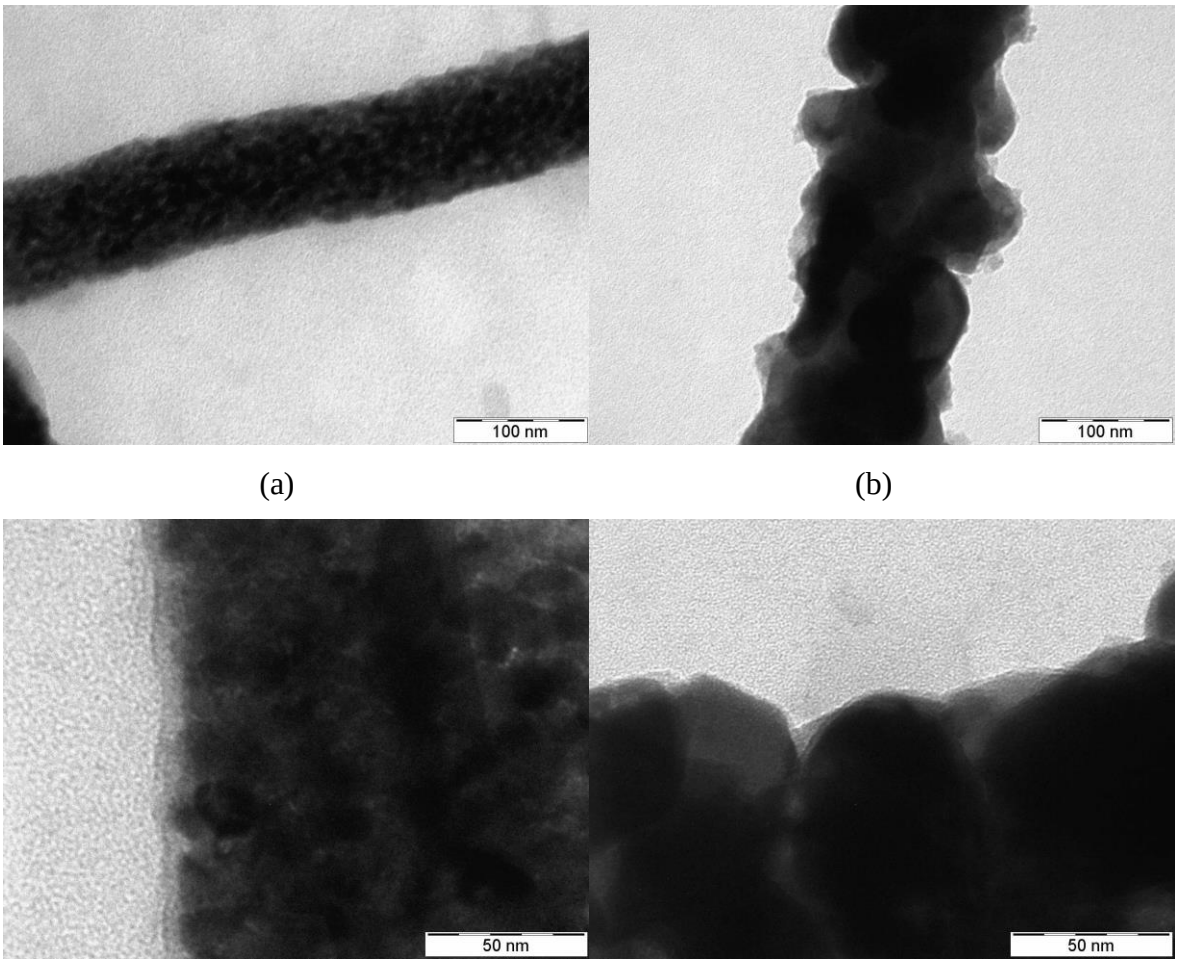

(a) (b)

(c) (d)

Fig. 4.

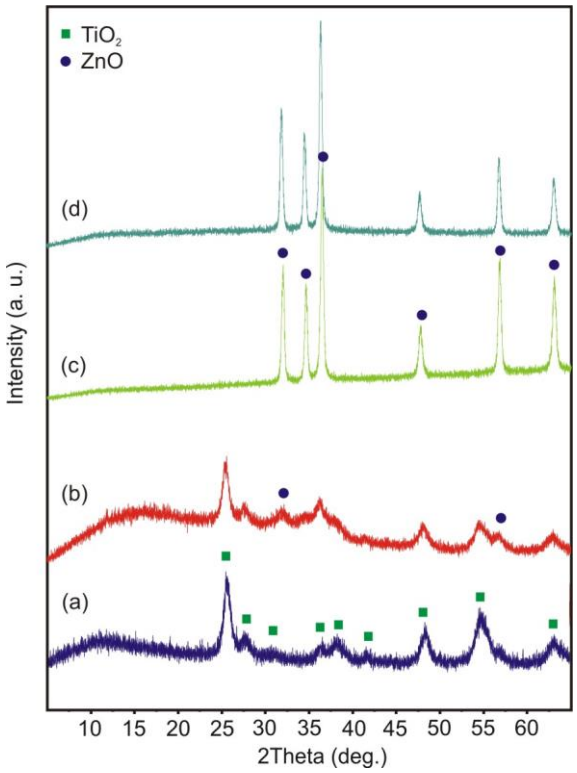
TiO2
ZnO
(d)
(c)
(b)
(a)
Intensity (a. u.)
10 15 20 25 30 35 40 45 50 55 60
2Theta (deg.)

Fig. 5.

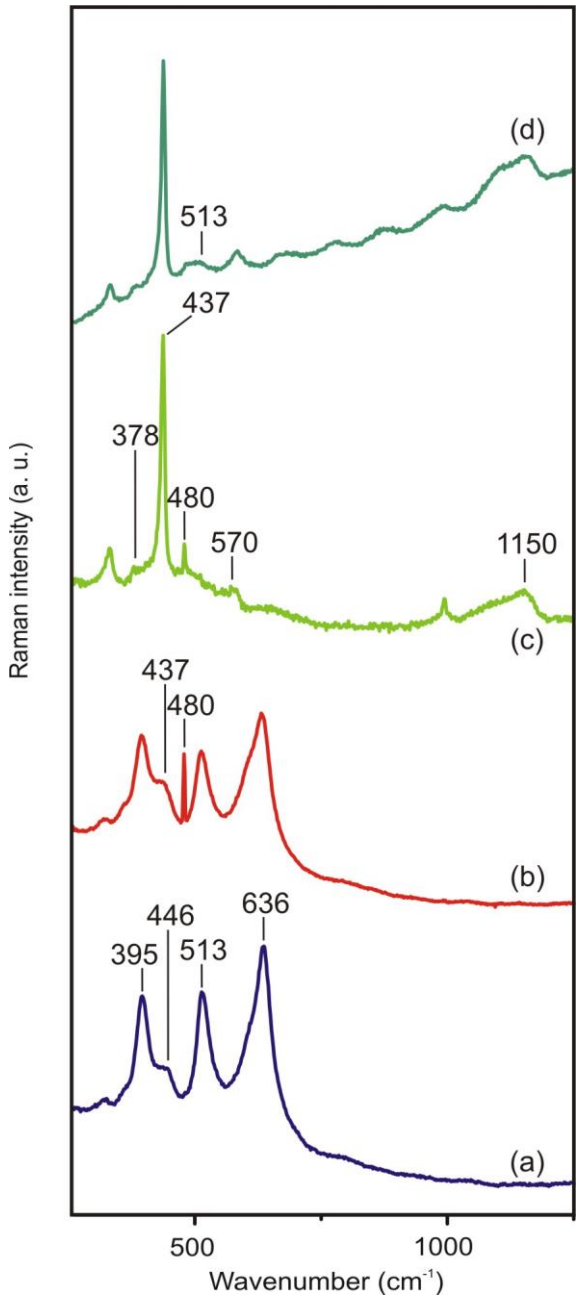
(d)
513
437
378
480
570
1150
(c)
437
480
(b)
446
636
395
513
(a)
Raman intensity (a. u.)
500
1000
Wavenumber (cm-1)

Fig. 6.

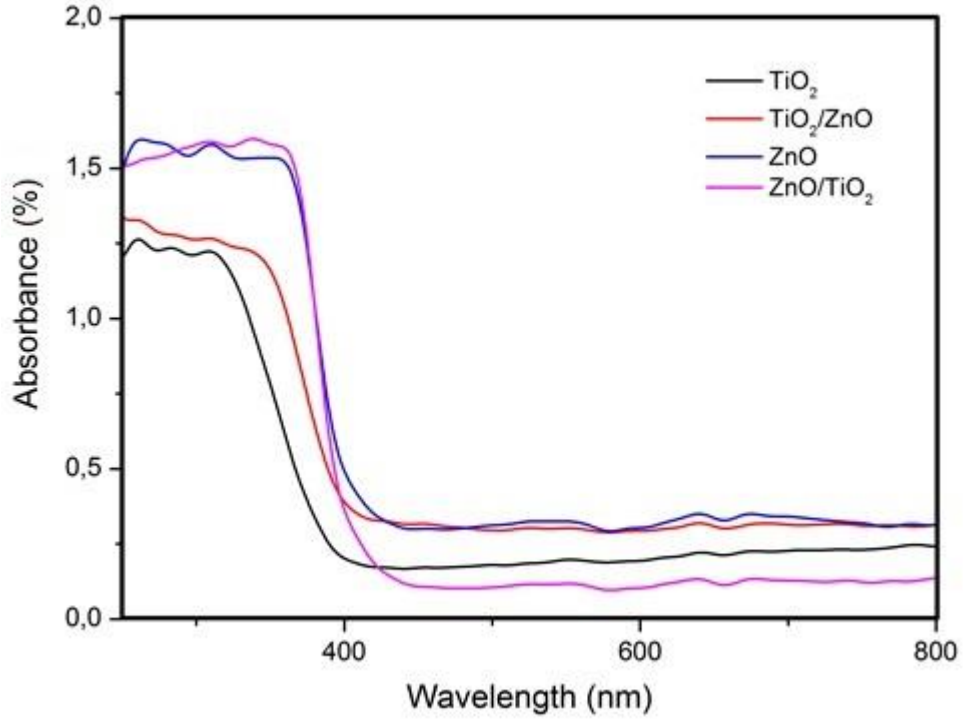
2,0
1,5
1,0
0,5
0,0
Absorbance (%)
400
600
800
Wavelength (nm)
TiO2
TiO2/ZnO
ZnO
ZnO/TiO2

Fig. 7.

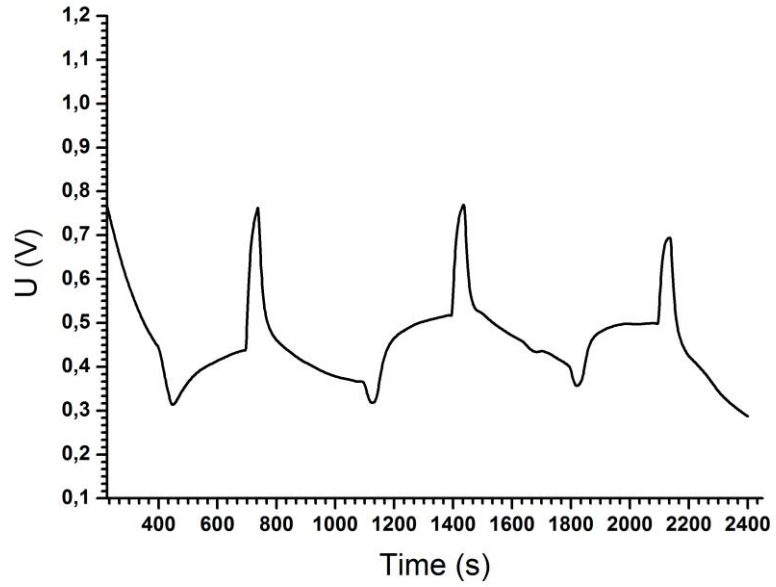
1,2
1,1
1,0
0,9
0,8
0,7
0,6
0,5
0,4
0,3
0,2
0,1
U (V)
400
600
800
1000
1200
1400
1600
1800
2000
2200
2400
Time (s)

(a)

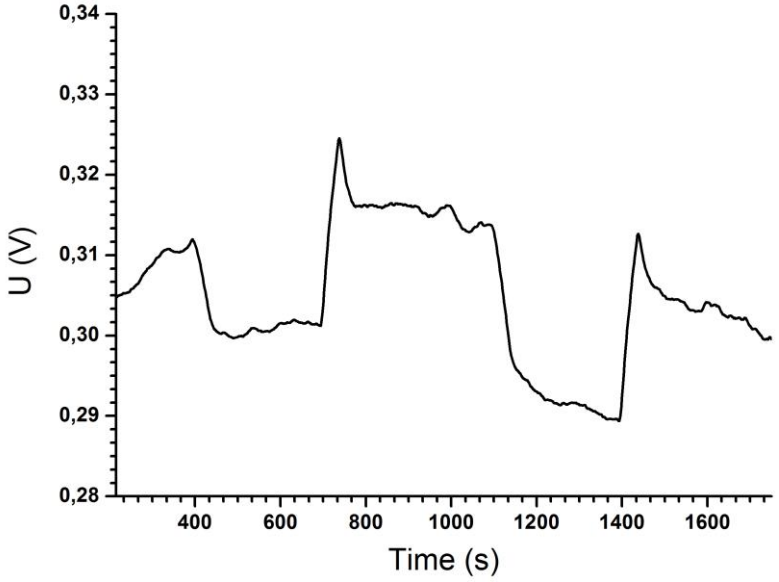
0,34
0,33
0,32
0,31
0,30
0,29
0,28
U (V)
400
600
800
1000
1200
1400
1600
Time (s)

(b)

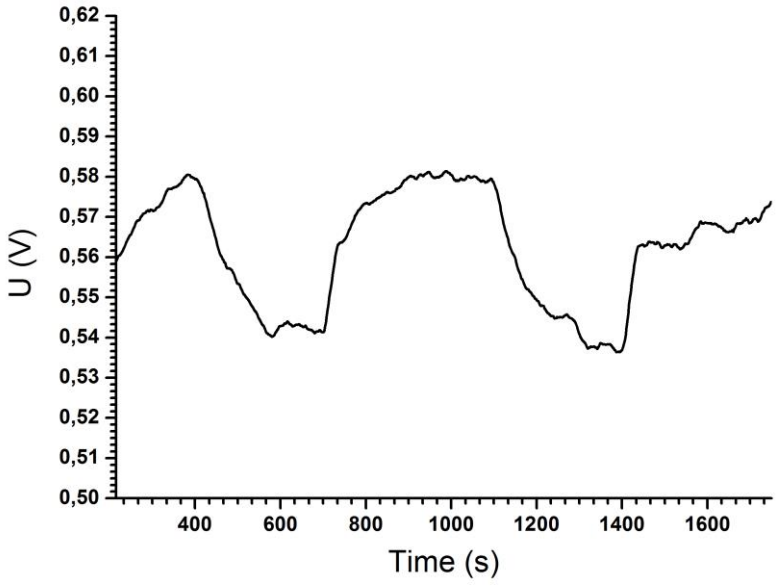
0,62
0,61
0,60
0,59
0,58
0,57
0,56
0,55
0,54
0,53
0,52
0,51
0,50
U (V)
400
600
800
1000
1200
1400
1600
Time (s)

(c)

Fig. 8.

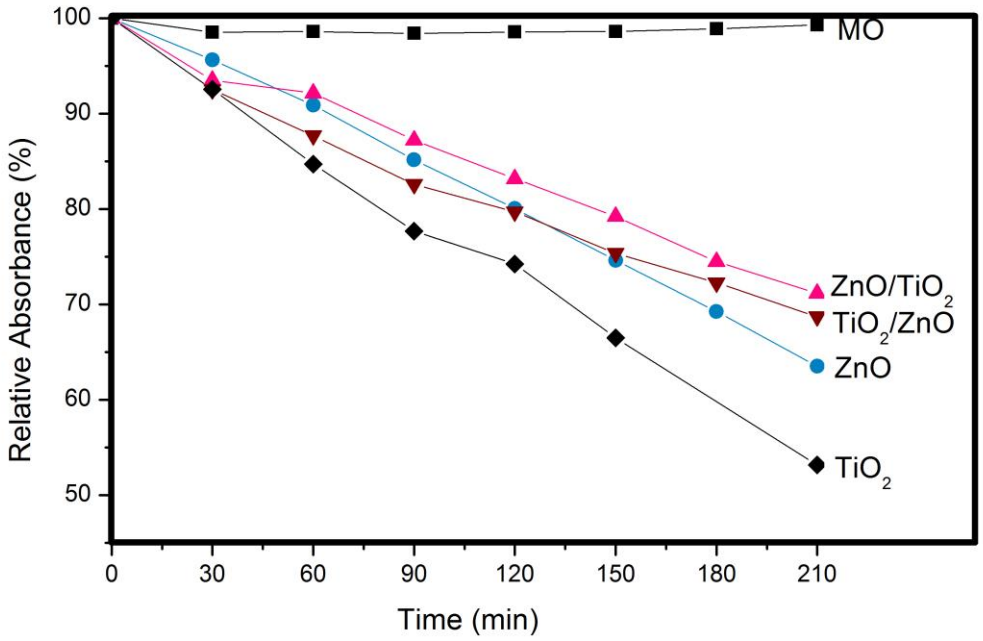
Relative Absorbance (%)
100
90
80
70
60
50
0
30
60
90
120
150
180
210
Time (min)
MO
ZnO/TiO2
TiO2/ZnO
ZnO
TiO2

Fig. 9.